2026 IEEE/SICE International Symposium on System Integration (SII)
January 11-14, 2026. Cancún, México

Simulation-Based Evaluation of a Shape-Transformable Autonomous Surface Robot Switching between Traveling and Station-Keeping Modes

Yasuyuki Fujii[1] and Joo-Ho Lee[1]

Abstract— **This paper presents a simulation-based evaluation of Intelligent WAter Knowledge Observer-8 (BIWAKO-8), a compact autonomous surface robot equipped with a transformable locomotion mechanism that switches between the Station-keeping mode and the Straight-travel mode. A Webots-based simulation environment replicating field conditions was used to compare the two modes under four settings: ideal, disturbance-only, localization-error-only, and a realistic combination. Across all settings, the Straight-travel mode completed missions faster, whereas the Station-keeping mode consistently consumed less energy, revealing a clear speed–energy trade–off. Disturbances had negligible impact on the energy efficiency of the Straight-travel mode, while localization error increased energy use in both modes by inducing more frequent heading corrections. These findings support hybrid operation—using the Straight-travel mode for transit and the Station-keeping mode for precise positioning—as an effective strategy for long-duration autonomous surface missions.**

I. INTRODUCTION

In recent years, large-scale environmental changes have been observed globally, exerting substantial impacts on aquatic environments such as seas and lakes. To analyze these impacts and assess their implications for fisheries and global ecosystems, extensive research and development efforts have been devoted to autonomous surface and underwater robotic platforms [1], [2]. These platforms have been utilized in diverse applications, including infrastructure inspection and maintenance near aquatic environments, environmental monitoring, and even entertainment-oriented surface mobility [3]–[6].

A major challenge for Autonomous Surface Vehicles (ASVs) is their limited continuous operation time, primarily constrained by onboard energy capacity. Numerous studies have addressed this limitation through control-based strategies such as energy-efficient trajectory planning and flow-aware control [7]–[9], as well as through energy-harvesting approaches exploiting solar or wind power [10], [11]. In contrast, this study tackles the energy problem from a mechanical perspective—by improving the locomotion mechanism itself. The proposed system enhances energy efficiency by switching between a disturbance-resistant Station-keeping mode and a low-drag Straight-travel mode according to mission requirements.

Our research group has developed compact autonomous surface robots designed for long-term, continuous water-quality monitoring over wide aquatic areas, with the goal of analyzing environmental changes and their potential impacts on human life [12]–[15]. However, conventional boat-shaped or hull-type ASVs with line-symmetric designs often struggle to maintain position under uncertain and varying disturbances, since their propulsion systems are not optimized for multi-directional thrust generation. To overcome this limitation, we developed the Brief Intelligent WAter Knowledge Observer-X (BIWAKO-X), an X-shaped, point-symmetric autonomous surface robot specialized for stationary environmental observation. This configuration provides high robustness against disturbances of varying directions and magnitudes, enabling reliable station-keeping performance in both field and simulation experiments.

Previous studies have proposed and validated, through simulation and real-world experiments, station-keeping strategies to reduce energy consumption under irregular environmental disturbances (e.g., waves and wind) and patrolling strategies for efficient multi-point observation [12]. The X-shaped locomotion mechanism used in these works offers a key advantage for station-keeping: regardless of the disturbance direction, the vehicle can promptly generate thrust to restore its position. However, in multi-point patrolling tasks that require straight-line travel between observation points, this configuration faces two major drawbacks: (*i*) large form drag during forward motion and (*ii*) underutilization of available thrust due to non-optimal orientation.

To overcome these issues, we developed a novel transformable locomotion mechanism that can switch between two configurations: (1) a Station-keeping mode, retaining the multi-directional disturbance resistance of the X-shaped design, and (2) a Straight-travel mode, in which the arm links are reconfigured to reduce form drag and align the thrusters with the travel direction, improving propulsion efficiency [16]. Field experiments demonstrated the feasibility of this mechanism in natural aquatic environments. However, since disturbance conditions vary over time, fair performance comparisons between configurations under identical conditions remain challenging.

To address this limitation, the present study develops a Webots-based simulation environment that replicates realistic field disturbances and localization errors, enabling systematic and fair evaluation of the transformable locomotion mechanism. The main contributions of this study are as follows:

- Development of a Webots-based simulation environment that incorporates realistic disturbances and localization errors, allowing fair and repeatable comparisons between locomotion modes.
- Quantitative analysis of a shape-transformable au-

[1]College of Information Science and Engineering, Ritsumeikan University, Japan.fujiyasu@fc.ritsumei.ac.jp

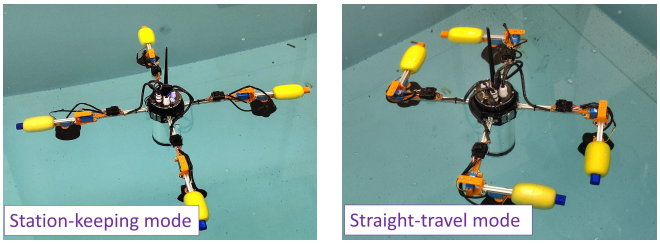

(a) Station-keeping mode (b) Straight-travel mode

Fig. 1: Overall appearance of BIWAKO-8 in the two locomotion modes: (a) Station-keeping mode, where the thrusters are oriented for omnidirectional thrust generation, and (b) Straight-travel mode.

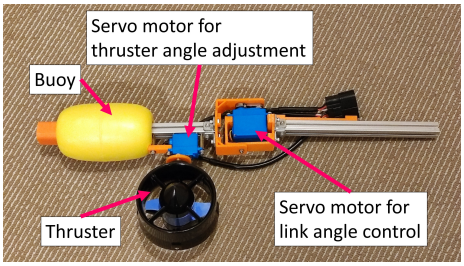

Fig. 2: Configuration of the thruster arm used in the transformable locomotion mechanism of BIWAKO-8. The arm integrates a thruster, buoy, and two servo motors for link-angle control and thruster-angle adjustment, enabling reorientation between the Station-keeping and Straight-travel modes.

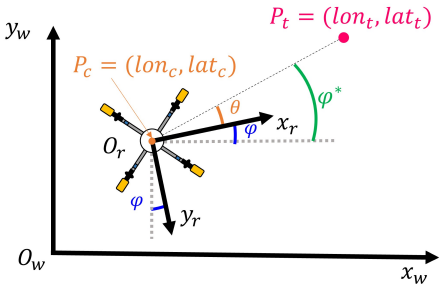

Fig. 3: Coordinate system

tonomous surface robot across station-keeping and straight-travel modes under four environmental conditions, clarifying the trade-off between mission time and energy consumption.

Accordingly, this study investigates the effectiveness of the Straight-travel mode relative to the Station-keeping mode in multi-point patrolling tasks, based on quantitative comparisons under identical simulated disturbance conditions.

II. BIWAKO-8

This section presents the configuration, control methodology, and locomotion algorithm of BIWAKO-8 (Brief Intelligent WAter Knowledge Observer-8), a compact autonomous surface robot equipped with a transformable locomotion mechanism [16]. Fig. 1 provides an overview of the BIWAKO-8.

A. Configuration

BIWAKO-8 comprises two main subsystems: a control unit housing the onboard computer and power supply, and a transformable locomotion mechanism integrating thrusters, servo-driven joints, and buoyant floats. An overview of the platform is shown in Fig. 1.

1) Control Unit: The control unit integrates a Raspberry Pi 3 Model B+ as the main control computer and a Navio 2 flight controller equipped with a Global Navigation Satellite System (GNSS) receiver and a nine-axis Inertial Measurement Unit (IMU). These sensors provide latitude, longitude, angular velocity, acceleration, and heading data required for real-time state estimation. Propulsion commands are executed via an Electronic Speed Controller (ESC) that drives the thrusters using Pulse Width Modulation (PWM) signals. A PCA9685-based servo driver controls the joints of the transformable mechanism. Power is supplied by a sealed three-cell Lithium Polymer (LiPo) battery (11.1 V, 6,000 mAh), which, along with all electronic modules, is enclosed in a waterproof compartment to ensure reliable operation in aquatic environments.

2) Transformable Locomotion Mechanism: The transformable locomotion mechanism enables the robot to switch between two optimized configurations: (*i*) Station-keeping mode (Fig. 1a), where the arm links and thruster orientations are arranged to maximize omnidirectional thrust generation, allowing rapid correction against environmental disturbances; and (*ii*) Straight-travel mode (Fig. 1b), where the arm geometry is reconfigured to reduce form drag and the thrusters are rotated by $45°$ to align with the travel direction, improving propulsion efficiency.

Each transformable arm module integrates a thruster, two servo motors, and a buoyant float. One servo motor controls the link angle between the arm and the main body, while the other adjusts the thrust direction by rotating the thruster. The overall geometry of the arm is illustrated in Fig. 2. A float is attached to the distal end of each arm to enhance buoyancy and generate restoring torque, contributing to the robot's stability on the water surface. Bidirectional thrusters provide both forward and reverse thrust, enabling precise maneuvering under various environmental conditions.

B. Control Method

1) Coordinate Systems: Fig. 3 illustrates the relationship between the robot coordinate frame (O_r, x_r, y_r) and the world coordinate frame (O_w, x_w, y_w). The current position $P_c = (lon_c, lat_c)$ and the target position $P_t = (lon_t, lat_t)$ are defined in the world frame.

2) Control in Station-keeping Mode: In Station-keeping mode, the robot selects one of eight movement directions (D_1–D_8) based on the relative angle θ between its current heading φ and desired heading φ^* (Eq.(1)). As shown in Fig. 4, each θ range corresponds to a specific direction D_i. When a diagonal direction (D_2, D_4, D_6, or D_8) is

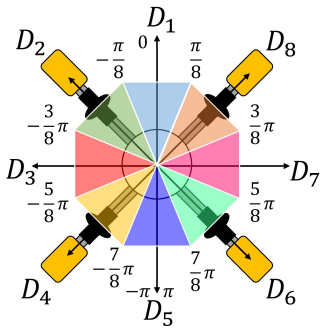

Fig. 4: Mapping between the relative angle θ to the target direction and the discrete movement directions D_1–D_8 used in the Station-keeping mode. Each colored sector represents the range of θ assigned to a corresponding direction D_i, and the arrows illustrate the resultant thrust orientations of the four thrusters for omnidirectional position control.

TABLE I: Thrust-coefficient settings for the straight-travel mode: command vectors $\boldsymbol{\tau} = [\tau_1, \tau_2, \tau_3, \tau_4]$.

Relative angle θ	τ_1	τ_2	τ_3	τ_4
$0 \le \theta < \frac{\pi}{2}$	1	$-\tau_s$	-1	1
$\frac{\pi}{2} \le \theta < \pi$	1	-1	$-\tau_s$	1
$-\pi \le \theta < -\frac{\pi}{2}$	1	-1	-1	τ_s
$-\frac{\pi}{2} \le \theta < 0$	τ_s	-1	-1	1

chosen, only the two thrusters required for lateral force generation are activated, reducing power consumption while maintaining positional stability. No explicit hysteresis band was introduced between direction sectors, as the switching logic is evaluated at discrete time steps (0.1 s) and no boundary oscillation was observed in the simulation results.

$$\varphi^* = \frac{\pi}{2} + \text{atan2}\left(\sin(\Delta lon_t)\cos(lat_t),\right.$$
$$\left.\cos(lat_c)\sin(lat_t) - \sin(lat_c)\cos(lat_t)\cos(\Delta lon_t)\right) \quad (1)$$

3) Control in Straight-travel Mode: In Straight-travel mode, all four thrusters (T_1—T_4, Fig. 5) are actively controlled to maintain the desired heading while propelling the robot toward a target waypoint. The relative angle to the waypoint, denoted as θ, and its rate of change $\dot{\theta}$ are input to a proportional-–derivative (PD) controller that determines the steering demand. The control strategy utilizes only the front-side thrusters for differential thrusting, allowing simultaneous heading correction and propulsion with minimal power consumption.

The thrust coefficient vector $\boldsymbol{\tau} = [\tau_1, \tau_2, \tau_3, \tau_4]^T$ is selected based on the quadrant of the heading direction, as summarized in TABLE I. Each element τ_i corresponds to the thrust weighting factor for the i-th thruster (T_1–-T_4), where a positive or negative sign indicates the direction of thrust output. The asymmetric gain parameter $\tau_s \in [0.5, 1]$, which modulates the contribution of the front thrusters, is computed using Eq. (2):

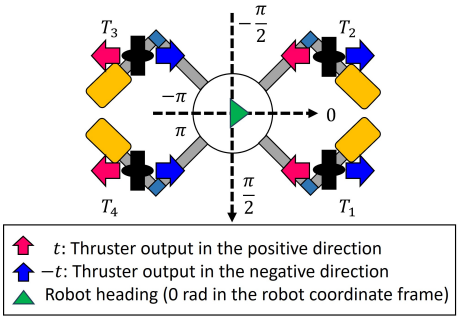

Fig. 5: Straight-travel mode thruster configuration of BIWAKO-8. Thrusters T_1—T_4 are rotated by 45° to align their thrust vectors with the forward direction (0 rad), enabling efficient straight-line propulsion.

$$\theta_e(t) = \begin{cases} |\pi - \theta(t)|, & 0 \le \theta(t) < \frac{\pi}{2} \\ |\theta(t) + \pi|, & -\pi \le \theta(t) < -\frac{\pi}{2} \\ |\theta(t)|, & -\frac{\pi}{2} \le \theta(t) < 0 \\ \theta(t), & \text{otherwise} \end{cases}$$
$$\dot{\theta}_e(t) = \frac{\theta_e(t) - \theta_e(t - \Delta t)}{\Delta t}$$
$$u_\theta(t) = K_\theta^P \cdot \theta_e(t) - K_\theta^D \cdot \dot{\theta}_e(t)$$
$$\tau_s(t) = \max\left(\min\left(1 - \frac{2u_\theta(t)}{\frac{\pi}{2}}, 1\right), 0.5\right) \quad (2)$$

This formulation ensures a smooth transition between aggressive and conservative turning depending on the relative heading. The proposed method allows simultaneous heading correction and straight-line travel, improving navigational efficiency toward distant goals.

4) Thruster Command Control: The final control input for each thruster is determined based on the distance to the current target. Specifically, the geodesic distance d between the current position P_c and the target waypoint P_t is computed, and a PD controller is applied to adjust the total thrust magnitude u_d:

- When d is large, u_d increases to enable rapid movement toward the target.
- As d decreases, u_d is proportionally reduced, enabling smooth deceleration and precise stopping at the waypoint.

The total thrust input u is defined as:

$$u = u_d \sum_{n=1}^{4} |\tau_n|$$

where $\boldsymbol{\tau}$ is the thrust coefficient vector described in TABLE I. The computation of d and u_d is presented in Eq. (3):

$$d(t) = \text{geodesic}(P_c, P_t)$$
$$\dot{d}(t) = \frac{d(t) - d(t - \Delta t)}{\Delta t}$$
$$u_d(t) = K_d^P \cdot d(t) - K_d^D \cdot \dot{d}(t) \quad (3)$$

C. Locomotion Algorithm

The patrolling mission consists of visiting a sequence of predefined waypoints in order. This framework enables direct performance comparisons under identical mission conditions in simulation and field trials.

III. Simulation Experiments

This section describes the simulation-based evaluation of the proposed transformable locomotion mechanism using the Webots robot simulator [17]. A virtual environment replicating the real-world experimental field was constructed, and BIWAKO-8 was tasked with patrolling multiple waypoints under different operating conditions. Performance was compared between the Station-keeping mode and the Straight-travel mode in terms of total energy consumption and mission completion time. The objective of this experiment is to quantitatively verify the operational advantages of the transformable mechanism under realistic environmental disturbances and localization errors, using a reproducible simulation environment specifically developed for this study

A. Experimental Conditions

In the simulation environment, four waypoints specified by latitude-–longitude coordinates were placed at the corners of a $100\ \mathrm{m} \times 100\ \mathrm{m}$ square. Starting from the initial location, BIWAKO-8 visited each waypoint sequentially in the predefined order. To reduce random variability and obtain representative performance metrics, the robot completed three full loops of the course in each trial, and the recorded values were averaged over the entire run. A waypoint was considered reached when the robot entered a circular area of radius $3.0\ \mathrm{m}$ centered on the waypoint.

The total energy consumption E was computed using Eq. (4), where A, P, and E denote the current, instantaneous power, and cumulative energy consumption, respectively, and Δt is the sampling period. The current was estimated from the thruster output using parameters obtained in preliminary experiments, assuming the rated voltage of the real BIWAKO-8 platform (12 V). The sampling frequency was fixed at 10 Hz, matching the physical system.

$$\begin{aligned} A &= \frac{3}{2} \cdot \frac{u_d}{u_{d,\max}} \cdot \sum_{n=1}^{4} |\tau_n|^2 \\ P &= 12A \\ E &= \sum P\,\Delta t \end{aligned} \tag{4}$$

The current A was modeled as proportional to the squared thrust coefficients, as shown in Eq. (4), to reflect the empirical relationship between motor load and commanded thrust observed in prior bench tests. Although simplified, this model reproduces the relative trends of power consumption observed in field operations. The sampling frequency was fixed at 10 Hz, matching the physical system.

1) Control gain settings: The PD gains used for heading and distance control were determined via a dedicated tuning simulation. In this environment, BIWAKO-8 repeatedly performed a simplified task of approaching a fixed target from varying initial poses and distances, under nominal conditions without external disturbances. For heading control, the proportional and derivative gains were set to $K_\theta^P = 0.3$ and $K_\theta^D = 2.0$, enabling fast and stable convergence to the desired heading. For thrust magnitude modulation based on distance, $K_d^P = 1.5$ and $K_d^D = 3.0$ were selected to balance rapid movement and smooth deceleration. These gain values were fixed throughout all main simulation experiments and were selected to minimize energy consumption while ensuring reliable arrival at waypoints.

To approximate real-world disturbances, the following two factors were introduced:

2) External disturbance: A horizontal drift velocity disturbance was applied in both the north (Y-axis) and east (X-axis) directions of the world frame. For each direction, the drift velocity was randomly drawn from a uniform distribution in the range $[-0.2,\ 0.2]\ \mathrm{m/s}$, corresponding to a maximum possible drift speed of $0.2\ \mathrm{m/s}$. The disturbance values in both directions were re-sampled every $300\ \mathrm{s}$ (5 minutes), independently for the northward and eastward components, to emulate temporally varying wind- or current-induced drift. The upper limit of $0.2\ \mathrm{m/s}$ was empirically set based on prior field experience with BIWAKO-8 under moderate wind and surface-current conditions.

3) Localization error: Gaussian noise with zero mean and standard deviation $\sigma = 1.5\ \mathrm{m}$, temporally correlated with coefficient $\rho = 0.9$ to simulate drift-like GPS error via a first–order Gauss-–Markov process:

$$a_k = \begin{cases} w_0, & k = 0, \\ \rho\, a_{k-1} + \sqrt{1-\rho^2}\, w_k, & k \geq 1, \end{cases}$$
$$w_k \sim \mathcal{N}(0, \sigma^2),$$

where w_k is zero-mean Gaussian noise with variance σ^2. The `accuracy` and `noiseCorrelation` parameters of the Webots GPS node were set accordingly. The parameters $\sigma = 1.5\ \mathrm{m}$ and $\rho = 0.9$ were empirically chosen based on prior field experience with localization performance in lake environments.

Based on these factors, four experimental conditions were defined:

- I No external disturbance and no localization error (baseline),
- II External disturbance only,
- III Localization error only,
- IV Both external disturbance and localization error.

Each condition was tested under two operating modes of BIWAKO-8: Station-keeping mode and Straight-travel mode. In the later discussion and in Fig. 7, the notation "Station-keeping mode (a)" refers to the trajectory obtained under condition I in Station-keeping mode, while "Straight-travel mode (d)" refers to the trajectory under condition IV in Straight-travel mode, and so forth.

B. Experimental Results

1) Baseline Potential and Realistic Scenario: Under the baseline condition (no disturbance, no localization error),

TABLE II: Experimental results for each locomotion mode and condition. Energy consumption is cumulative over the mission, and mission time is the total duration to visit all waypoints.

Locomotion mode	Condition	Energy consumption (kJ)	Mission time (s)
Station-keeping	I	87.81	1807.50
	II	104.67	2140.30
	III	90.90	1737.20
	IV	95.21	1948.30
Straight-travel	I	95.42	1418.80
	II	104.89	1586.90
	III	98.81	1494.30
	IV	105.64	1590.60

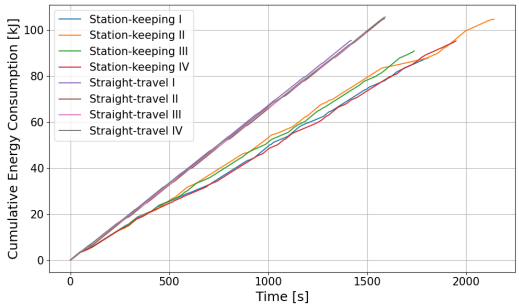

Fig. 6: Cumulative energy E [kJ] vs. time [s] under four settings (ideal, disturbance-only, localization-error-only, combined), comparing station-keeping and straight-travel.

which evaluates the intrinsic potential of each locomotion mode, the Straight-travel mode reduced mission time by 21.50% compared to Station-keeping, at the cost of an 8.66% increase in energy consumption. In the realistic scenario (disturbance + localization error), Straight-travel mode shortened mission time by 18.36% but increased energy consumption by 10.95%, indicating a clear trade–off between speed and energy efficiency in real-world conditions.

2) Other Environmental Variations: In the disturbance-only condition, Straight-travel mode achieved a 25.86% reduction in mission time with a negligible 0.21% increase in energy, showing strong robustness against disturbances. In the localization-error-only condition, mission time was reduced by 13.98% with an 8.71% energy increase, suggesting that frequent heading corrections due to error are more costly for Straight-travel mode. Although disturbance-free and error-free operation may occasionally occur in real-world missions, the realistic scenario results indicate that time savings from Straight-travel mode often come at the expense of higher energy usage.

3) Trajectories: Fig. 7 illustrates representative trajectories for each condition, with waypoints visited in the fixed order (red, blue, green, purple). Without disturbance and error (Condition I), both modes produced direct waypoint–to–waypoint motion; the Station-keeping mode exhibited small oscillations due to its geometry and control characteristics. Under disturbance (Condition II), both modes performed heading corrections to reach targets, with the Station-keeping mode showing larger oscillations around the desired path. Localization error (Condition III) introduced additional deviations and small loops in both modes, yet all missions were completed. In the realistic setting (Condition IV), the Straight-travel mode paths remained comparatively direct, whereas the Station-keeping mode showed more pronounced lateral excursions and oscillations.

IV. Discussion

The simulation results show that the Straight-travel mode generally completes missions faster, while the Station-keeping mode consumes less energy. This contrast stems from design differences: the Straight-travel mode achieves higher speed but requires frequent thrust adjustments under disturbances or localization errors, whereas the Station-keeping mode uses fewer thrusters, reducing power but slowing travel.

Under combined disturbance and localization error, the Straight-travel mode maintains speed at the cost of higher energy use, indicating a clear speed–energy trade-off. Thus, time-critical missions (e.g., wide-area surveys) benefit from the Straight-travel mode, while energy-limited, long-duration operations favor the Station-keeping mode.

Disturbance alone had little effect on the Straight-travel mode's efficiency, showing robustness to environmental forces. In contrast, localization errors caused oscillatory corrections that increased energy use in both modes. Improving localization, adapting speed, or switching modes near waypoints could retain the Straight-travel mode's speed advantage while narrowing the energy gap.

Overall, the results highlight that optimal BIWAKO-8 operation should balance time and energy efficiency as complementary objectives.

V. Conclusion

This study evaluated the effectiveness of a transformable locomotion mechanism for a compact autonomous surface robot through simulation experiments. Using a Webots-based environment enabled performance assessment under controlled and repeatable conditions that are challenging to achieve in the field. The results showed that the Straight-travel mode consistently shortened mission completion time, while the Station-keeping mode generally required less energy, revealing a clear trade–off between speed and energy efficiency in realistic conditions. Disturbance had little effect on the energy efficiency of the Straight-travel mode, whereas localization error increased energy demand in both modes due to oscillatory heading corrections.

Future work includes exploring hybrid strategies that combine the Straight-travel mode for transit with the Station-keeping mode for precise positioning, followed by validation of these strategies in real-world field experiments.

Acknowledgement

This research was conducted with the support of a research grant from The Mazda Foundation.

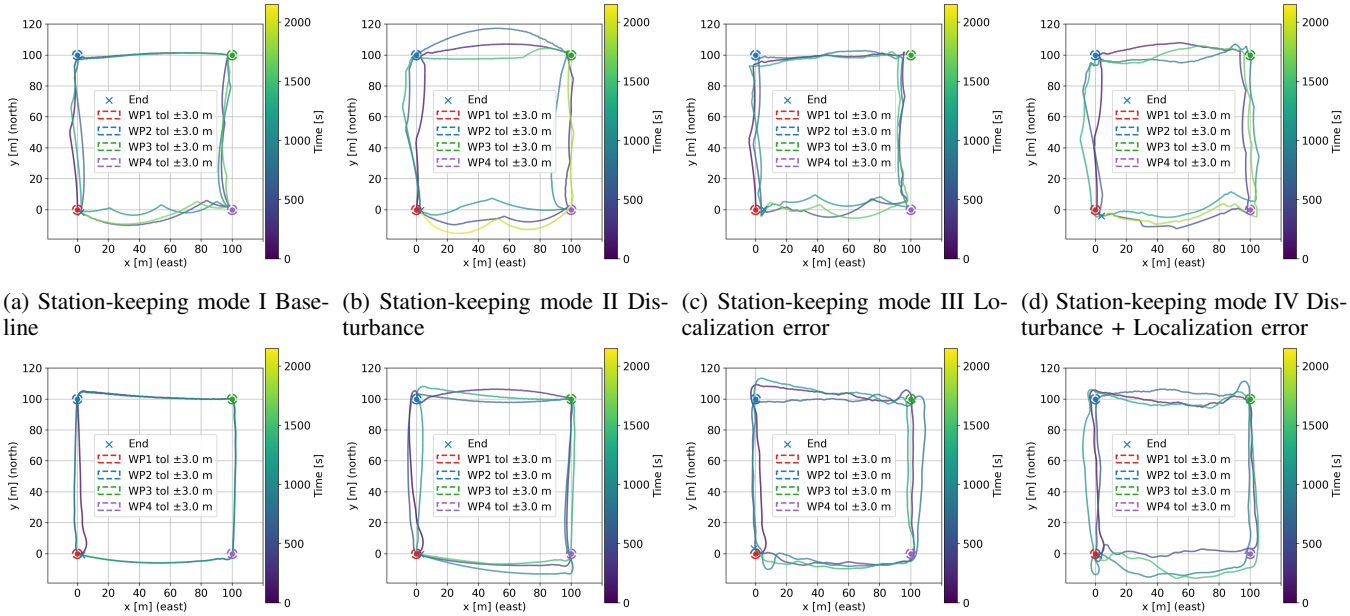

(a) Station-keeping mode I Baseline (b) Station-keeping mode II Disturbance (c) Station-keeping mode III Localization error (d) Station-keeping mode IV Disturbance + Localization error

(e) Straight-travel mode I Baseline (f) Straight-travel mode II Disturbance (g) Straight-travel mode III Localization error (h) Straight-travel mode IV Disturbance + Localization error

Fig. 7: Trajectories of BIWAKO-8 under two operating modes and four experimental conditions. Subfigures (a)–(d) show the Station-keeping mode, and subfigures (e)–(h) show the Straight-travel mode. Each subfigure corresponds to one of the following conditions: I — Baseline (no external disturbance and no localization error); II — Disturbance only; III — Localization error only; IV — Disturbance + Localization error. Color encodes time (0–2150 s). Waypoints WP1–WP4 are at $(0, 0)$, $(0, 100)$, $(100, 100)$, and $(100, 0)$ with 3 m tolerance circles in the local frame (x east, y north).

REFERENCES

[1] F. Nekovář, J. Faigl, and M. Saska, "Multi-vehicle dynamic water surface monitoring," *IEEE Robotics and Automation Letters*, vol. 8, no. 10, pp. 6323–6330, 2023.

[2] S. Manjanna, A. Q. Li, R. N. Smith, I. Rekleitis, and G. Dudek, "Heterogeneous multi-robot system for exploration and strategic water sampling," in *2018 IEEE International Conference on Robotics and Automation (ICRA)*. IEEE, 2018, pp. 4873–4880.

[3] K. Xue, X. Ji, D. Qu, Y. Peng, and H. Qian, "Oboat: An agile omnidirectional robotic platform for unmanned surface vehicle tasks," *IEEE/ASME Transactions on Mechatronics*, vol. 28, no. 5, pp. 2413–2424, 2023.

[4] W. Wang, D. Fernández-Gutiérrez, R. Doornbusch, J. Jordan, T. Shan, P. Leoni, N. Hagemann, J. K. Schiphorst, F. Duarte, C. Ratti, *et al.*, "Roboat iii: An autonomous surface vessel for urban transportation," *Journal of Field Robotics*, vol. 40, no. 8, pp. 1996–2009, 2023.

[5] W. Wang, T. Shan, P. Leoni, D. Fernández-Gutiérrez, D. Meyers, C. Ratti, and D. Rus, "Roboat ii: A novel autonomous surface vessel for urban environments," in *2020 IEEE/RSJ International Conference on Intelligent Robots and Systems (IROS)*. IEEE, 2020, pp. 1740–1747.

[6] S. Kong, M. Tian, C. Qiu, Z. Wu, and J. Yu, "Iwscr: An intelligent water surface cleaner robot for collecting floating garbage," *IEEE Transactions on Systems, Man, and Cybernetics: Systems*, vol. 51, no. 10, pp. 6358–6368, 2020.

[7] H. Homburger, S. Wirtensohn, P. Hoher, T. Baur, D. Griesser, M. Diehl, and J. Reuter, "Solgenia—a test vessel toward energy-efficient autonomous water taxi applications," *Ocean Engineering*, vol. 328, p. 121011, 2025.

[8] S. Wang, Y. Tuo, and D. Wang, "Weather optimal area-keeping control for underactuated autonomous surface vehicle with input time-delay," *International Journal of Naval Architecture and Ocean Engineering*, vol. 14, p. 100456, 2022.

[9] E. I. Sarda, H. Qu, I. R. Bertaska, and K. D. Von Ellenrieder, "Station-keeping control of an unmanned surface vehicle exposed to current and wind disturbances," *Ocean Engineering*, vol. 127, pp. 305–324, 2016.

[10] K. Sornek, J. Wiercioch, D. Kurczyna, R. Figaj, B. Wójcik, M. Borowicz, and M. Wieliński, "Development of a solar-powered small autonomous surface vehicle for environmental measurements," *Energy conversion and Management*, vol. 267, p. 115953, 2022.

[11] Q. Sun, W. Qi, H. Liu, Z. Sun, T. L. Lam, and H. Qian, "Oceanvoy: A hybrid energy planning system for autonomous sailboat," in *2020 IEEE/RSJ International Conference on Intelligent Robots and Systems (IROS)*. IEEE, 2020, pp. 2481–2487.

[12] Y. Fujii, D. T. Tran, and J.-H. Lee, "Multi-point traveling sensing strategy for a symmetrical shape autonomous on water surface robot," in *2024 IEEE/SICE International Symposium on System Integration (SII)*. IEEE, 2024, pp. 1235–1240.

[13] Y. Fujii, D. Tuan Tran, and J.-H. Lee, "An efficient in situ monitoring strategy for an active aquatic surface omni-directional sensing device," *Advanced Robotics*, pp. 1–15, 2022.

[14] Y. Fujii, K. Harada, H. Yamazoe, and J.-H. Lee, "Development and performance experiments in lake biwa of a small sensing device keeping fixed position on water," in *2020 17th International Conference on Ubiquitous Robots (UR)*. IEEE, 2020, pp. 494–499.

[15] Y. Fujii, H. Yamazoe, and J.-H. Lee, "A water sensing device control system for long-term monitoring," in *2019 IEEE/SICE International Symposium on System Integration (SII)*. IEEE, 2019, pp. 572–577.

[16] Y. Fujii, D. T. Tran, and J.-H. Lee, "Evaluation of an autonomous surface robot equipped with a transformable mobility mechanism for efficient mobility control," arXiv preprint arXiv:2508.08303, Aug 2025, presented at the ICRA 2025 Workshop on REaCT: Robotics for Environmental and Climate Assessment. [Online]. Available: https://arxiv.org/abs/2508.08303

[17] Webots, "http://www.cyberbotics.com," open-source Mobile Robot Simulation Software. [Online]. Available: http://www.cyberbotics.com